

AlGaAs–GaAs Quantum-Well Electrooptic Phase Modulator with Disorder Delineated Optical Confinement

Wallace C. H. Choy, Bernard L. Weiss, *Senior Member, IEEE*, and E. Herbert Li, *Senior Member, IEEE*

Abstract—Waveguide phase modulators, with 0.5- and 1- μm quantum-well (QW) active regions which are defined by impurity-induced disordering are investigated theoretically. By controlling the extent of the interdiffusion in the lateral claddings, the refractive index difference between the core and claddings is used to provide single-mode operation. Strong optical confinement, which is required to produce single-mode high-efficiency modulation, requires the peak impurity concentration to be at the center of the QW active region. Moreover, the annealing time needs to be optimized so that single mode can be maintained at the desired bias field. A low dopant concentration is also expected to minimize the destruction of the modulator structure. The results show that since the core/cladding interface is graded, the width of the metal contact is important. A comparison of modulation efficiency for active layer thicknesses of 0.5 and 1.0 μm shows that the 0.5- μm one is a more efficient structure and its absorption loss can be reduced by increasing the applied field from 50 to 100 kV/cm.

Index Terms—Electrooptic materials/devices, electrooptic modulation, optical losses, optical planar waveguides, quantum wells, semiconductor waveguides.

I. INTRODUCTION

THE III–V semiconductor quantum-well (QW) electrooptic phase modulators are of interest for a range of applications in optical communication and signal processing due to their large electrooptic effect [1], [2]. However, most QW phase modulators are discrete devices which are integrated with other devices to form photonic integrated circuits (PIC's). Impurity-induced disordering (IID) is a simple technology that is a candidate for the development of PIC's [3]. When impurities, such as Ga [4], Al [5], and O [6], or vacancies [7] are introduced selectively into a QW structure, such as by masked implantation, the rate of interdiffusion which is determined by the annealing temperature and time can be accelerated. Interdiffusion occurs across the well–barrier interface and modifies the transition energies, and thus the optical properties, which results in a change of refractive index between the as-grown and interdiffused QW regions [8]. This

process has been used to fabricate optical devices, such as lasers [9], modulators [10], and waveguides [11] on a single substrate and makes photonic integration a reality.

Conventional AlGaAs–GaAs QW modulators use the composition of the AlGaAs cladding layers to control the number of guided modes in the waveguide section of the modulator [12]. In this paper, the annealing time is used to control the extent of the interdiffusion, and therefore the refractive index change, to govern the modal characteristics of the waveguide modulator structure.

In this paper, we model an electrooptic phase modulator with lateral confinement provided by IID in an $\text{Al}_{0.3}\text{Ga}_{0.7}\text{As}$ –GaAs QW's active region. This paper addresses the effects of interdiffusion on the modulator performance and the waveguide characteristics of the modulator in terms of the thickness of the active region. The phase modulator is aimed as a single-mode waveguide device to reduce dispersion and achieve good performance. The results demonstrate the effects of structural parameters of the device and interdiffusion conditions on the modulator characteristics and shows how a useful phase modulator can be designed using interdiffusion.

II. MODELING OF THE PHASE-MODULATOR STRUCTURE

The structure of the phase modulator studied here is shown schematically in Fig. 1. Starting from the n^+ -GaAs substrate, the layers are an n^+ -type $\text{Al}_{0.3}\text{Ga}_{0.7}\text{As}$ lower cladding layer, a number of undoped quantum wells (QW's) consisting of 100- \AA $\text{Al}_{0.3}\text{Ga}_{0.7}\text{As}$ barriers and 100- \AA GaAs wells which serve as the active region of the device, and p^+ -type $\text{Al}_{0.3}\text{Ga}_{0.7}\text{As}$ upper cladding with metal contacts on the GaAs substrate and the upper cladding layer. IID is used to provide the lateral confinement in the active region of the modulator.

In order to investigate an ion-implanted phase modulator, a two-dimensional (2-D) diffused impurity profile of the QW active region and the corresponding refractive index profile are modeled. By solving the wave equation, the optical confinement of the waveguide structure is determined from the refractive index profile. The electrooptic and electroabsorption properties of the QW structure are then calculated. Several modulator parameters are determined to characterize the performance of the device. Besides the breakdown voltage characteristics, the effects of the applied voltage across the p-i-n structure are determined by solving the Poisson's equation.

Manuscript received May 19, 1997; revised September 4, 1997. This research work is supported in part by the University of Hong Kong, Committee on Research and Conference (CRGC). The work of W. C. H. Choy was supported by the Croucher Foundation.

W. C. H. Choy and B. L. Weiss are with the School of Electronic Engineering, Information Technology and Mathematics, University of Surrey, Guildford, Surrey, GU2 5XH, U.K.

E. H. Li is with the Department of Electrical and Electronic Engineering, University of Hong Kong, Pokfulam Road, Hong Kong.

Publisher Item Identifier S 0018-9197(98)00347-9.

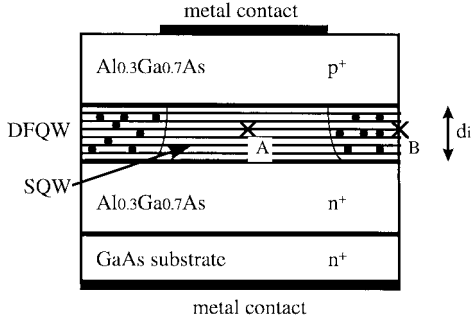


Fig. 1. The cross section of the waveguide-type phase modulator, where the guiding region contains square QW's after interdiffusion.

A. Optical Properties of QW

The real part of refractive index n_r , the imaginary part of refractive index, implies the absorption coefficient α , and the real and imaginary parts of the dielectric function, ε_1 and ε_2 , respectively, are the fundamental optical constants of the QW structure. The relationship between α and ε_2 is given by

$$\alpha(\omega) = \frac{\omega \varepsilon_2(\omega)}{c_0 n_r(\omega)} \quad (1)$$

where ω is the angular frequency and c_0 is the speed of light. This model of α has been described previously [13], [14] and is not the subject of the work reported here. The model for n_r is described in [15] and [16]. In the following, the important steps of modeling n_r are shown.

The dielectric functions are used to determine n_r and the relationship is given by

$$n_r(\omega) = \left(\frac{1}{2} \varepsilon_1(\omega) + \frac{1}{2} \{ [\varepsilon_1(\omega)]^2 + [\varepsilon_2(\omega)]^2 \}^{1/2} \right)^{1/2} \quad (2)$$

where ε_1 and ε_2 , the real and imaginary parts of the dielectric function, respectively, are given by

$$\varepsilon_1(\omega) = \varepsilon_1^\Gamma(\omega) + \varepsilon_1^L(\omega) + \varepsilon_1^X(\omega) + \varepsilon_\infty \quad (3)$$

$$\varepsilon_2(\omega) = \varepsilon_2^\Gamma(\omega) + \varepsilon_2^L(\omega) + \varepsilon_2^X(\omega) + \varepsilon_2^{\text{ID}} \quad (4)$$

where ε_1^Γ , ε_2^Γ denotes the contribution from the Γ valley, ε_1^L , ε_2^L denotes the contribution from L valley, ε_1^X , ε_2^X denotes the contribution from X valley, ε_∞ denotes the contribution from other transitions to ε_1 , while $\varepsilon_2^{\text{ID}}$ denotes the contribution from the indirect transitions to ε_2 . The quantum confinement affects the transitions contribution primarily in Γ valley and thus ε_1^Γ and ε_2^Γ while the contributions of bulk-like L and X valleys, and all other transitions above the QW to the real and imaginary dielectric functions, are obtained using bulk calculation [17].

By considering the effects contributed by QW layer and the bulk barrier layers, the imaginary part of the dielectric constant contributed by the Γ valley is derived

$$\varepsilon_2^\Gamma(\omega) = \varepsilon_2^{\text{exc}}(\omega) + \varepsilon_2^{\text{bound}}(\omega) + \varepsilon_2^{\Gamma_{\text{bulk}}}(\omega) \quad (5)$$

where the superscripts Γ , exc, bound, and Γ_{bulk} refer to the contributions of the Γ valley, the QW 1S bound exciton, the conduction-valence band QW bound state, and the contribution

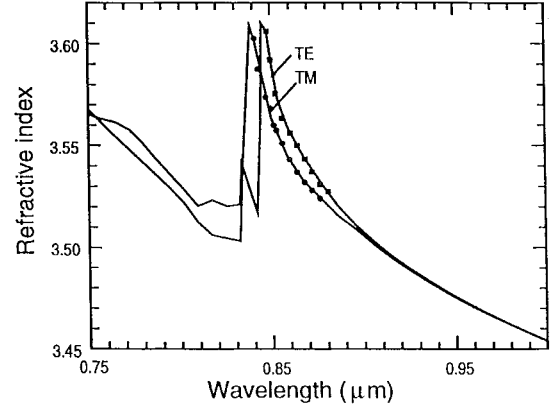


Fig. 2. Comparison of calculated TE and TM polarization refractive index spectra to experimental results of $\text{Al}_{0.26}\text{Ga}_{0.74}\text{As}$ -GaAs QW with well width of 80 Å. The experimental refractive indices taken from [18] are denoted by a filled square (TE) and a filled circle (TM).

due to the weighted AlGaAs barrier and GaAs well layers as a bulk material for the higher energy region without any quantum confinement effects, respectively. The expressions of $\varepsilon_2^{\text{exc}}$ and $\varepsilon_2^{\text{bound}}$ are taken from [13] together with (1), while $\varepsilon_2^{\Gamma_{\text{bulk}}}$ is taken from [17].

In the calculation of the as-grown square QW, the $\varepsilon_2^{\Gamma_{\text{bulk}}}(\omega)$ is calculated by weighting the barrier and well together in a ratio of well width (L_z) to barrier width (L_b)

$$\varepsilon_2^{\Gamma_{\text{bulk}}}(\omega) = [L_z \varepsilon_{2\text{well}}^{\Gamma_{\text{bulk}}}(\omega) + L_b \varepsilon_{2\text{barrier}}^{\Gamma_{\text{bulk}}}(\omega)] / (L_z + L_b). \quad (6)$$

For the case of a diffused QW, we divide each well and barrier layer into $n = 20$ subintervals and $\varepsilon_2^{\Gamma_{\text{bulk}}}(\omega)$ at each subinterval is calculated using the diffused Al concentration profile. The barrier layer $\varepsilon_2^{\Gamma_{\text{bulk}}}$ is then weighted with the well layer $\varepsilon_2^{\Gamma_{\text{bulk}}}$

$$\varepsilon_2^{\Gamma_{\text{bulk}}}(\omega) = (1/n) \sum_{i=1}^n \varepsilon_2^{\Gamma_{\text{bulk}}}(\omega)_i \quad (7)$$

where n is the number of subintervals in a barrier.

$\varepsilon_1^\Gamma(\omega)$ is determined using the Kramers-Kronig transformation of $\varepsilon_2^\Gamma(\omega)$, taking into consideration the well/barrier weighting [15]. The real part of the refractive index is evaluated from (2) by including the real and imaginary dielectric function contributions by the X and L valleys and higher order transitions obtained from a bulk calculation [17]. The calculated refractive index is compared with the experimental values taken from [18], as shown in Fig. 2. The result demonstrates a good agreement between the model and experiment. Under applied electric field, the change of refractive index is calculated by the Kramers-Kronig transformation from the change of absorption coefficient [19].

B. Disorder-Delineated QW Optical Waveguide

Lateral confinement of the active region is produced by Ga^+ implantation into the unmasked regions of the QW structure to provide enhanced interdiffusion after annealing. These interdiffused implanted regions have a lower refractive index than the masked unimplanted interdiffused regions so

that a waveguide is formed with the light being confined in the unimplanted region. Since the implanted ion concentration varies with depth in a controlled manner [20], the extent of the interdiffusion, and, thus, the refractive index depth profile, varies along the growth direction of the QW structure.

The theoretical model of implanted ion profile and the Al–Ga concentration profile after interdiffusion have been reported previously [21]. From the Al–Ga concentration profile, the corresponding diffusion length (L_d) is determined, where L_d is defined as $(Dt)^{1/2}$ and D and t are the interdiffusion coefficient and the annealing time, respectively. The effects of interdiffusion on the QW subband structure have been discussed previously [22] and are not the subject of the work reported here. Using the model discussed previously for n_x of interdiffused QW (DFQW) structures, a 2-D refractive index profile $n_x(x, y)$ is calculated for different L_d 's. By using the improved Fourier decomposition method [23], Maxwell's equations are solved to determine the waveguide characteristics of the phase modulator, including the number of guided modes and their propagation constants and the effective refractive indices.

C. Electrooptic and Electroabsorption Properties of the Modulator

Annealing the implanted structure modifies the impurity profile and results in a graded L_d profile between the waveguide core and cladding regions of the QW structure. The metal contacts are designed to cover the graded L_d regions, i.e., the active region is composed of DFQW's with different values of L_d (details later). Consequently, the electrooptic and electroabsorption properties of the modulator are obtained from DFQW's with different extents of interdiffusion. Under reverse bias, the optical properties, including absorption coefficient and refractive index, of these DFQW's change to produce the modulation characteristics.

The application of an external applied voltage tilts the QW's, red shifts the transition energies, and reduces the wavefunction overlap integrals (i.e., quantum-confined Stark effect). They result in a red shift of the exciton absorption peaks and reduce the peak absorption values, as shown in transverse electric mode (TE) absorption spectra [Fig. 3(a)]. The effective absorption coefficient, α_{eff} , is given by

$$\alpha_{\text{eff}} = \frac{\int_{\text{the wells within the active region}} \alpha(x, y) \varphi(x, y) \varphi^*(x, y) dA}{\int_{\text{the entire range of the guiding field}} \varphi(x, y) \varphi^*(x, y) dA} \quad (8)$$

where $\varphi(x, y)$ is the guiding optical field, dA is a small but finite area normal to the optical field at (x, y) , and $\alpha(x, y)$ is the absorption coefficient of the $\text{Al}_{0.3}\text{Ga}_{0.7}\text{As}$ –GaAs QW structure, since the extent of the interdiffusion in the QW region is inhomogeneous throughout the cross section of the phase modulation, i.e., the absorption is dependent on both x and y . Equation (8) shows that α_{eff} is determined by

the fraction of the optical field intensity $\varphi(x, y)\varphi^*(x, y)$ within the wells of active region. The field-induced change of effective absorption coefficient ($\Delta\alpha_{\text{eff}}$) in the device is calculated using:

$$\Delta\alpha_{\text{eff}} = \alpha_{\text{eff}}(F \neq 0) - \alpha_{\text{eff}}(F = 0) \quad (9)$$

where the $\alpha_{\text{eff}}(F \neq 0)$ and $\alpha_{\text{eff}}(F = 0)$ are the effective absorption coefficients with and without an applied field, respectively.

The TE refractive index spectra of the QW region and the change of refractive index due to different applied voltages are shown in Fig. 3(b) and (c), respectively. In Fig. 3(b), the refractive index reaches a heavy hole exciton peak at $0.852 \mu\text{m}$ and followed by a much smaller amplitude resonance which occurs at a slightly shorter wavelength at $0.843 \mu\text{m}$, due to the light hole. The waveguide effective refractive indices with and without an applied field are determined by solving Maxwell's equations using the refractive indices with the corresponding applied field which are then used to determine the change of the effective refractive index Δn_{eff} .

D. Modulation Characteristics

The important performance characteristics of the phase modulator are the phase change per unit modulation length per unit applied voltage, the chirp parameter, the optical confinement factor Γ , the absorption loss α_{loss} , and the required bias voltage.

The modulation efficiency of the phase modulator is measured from the phase change per unit modulation length per unit applied voltage, which is the normalized phase shift, $\Delta\theta_N$, and is given by

$$\Delta\theta_N = \frac{2\pi \Delta n_{\text{eff}}}{V(\text{applied}) \lambda_{\text{op}}} \quad (10)$$

where $V(\text{applied})$ is the applied voltage and λ_{op} is the operating wavelength. A high modulation efficiency requires a large $\Delta\theta_N$.

The static chirp parameter β_{mod} is given by

$$\beta_{\text{mod}} = \frac{4\pi \Delta n_{\text{eff}}}{\lambda_{\text{op}} \Delta\alpha_{\text{eff}}} \quad (11)$$

where both $\Delta\alpha_{\text{eff}}$ and Δn_{eff} are functions of the applied voltage [19]. Equation (11) shows that β_{mod} can be considered as a measure of the phase modulation strength to intensity modulation strength due to an applied electric field. A useful phase modulator requires chirp parameter >10 [24].

The optical confinement factor Γ is determined using

$$\Gamma = \frac{\int_{\text{the depletion region of the waveguide device}} \varphi(x, y) \varphi^*(x, y) dA}{\int_{\text{the entire cover range of a guiding field}} \varphi(x, y) \varphi^*(x, y) dA} \quad (12)$$

where the Γ parameter indicates the portion of the optical

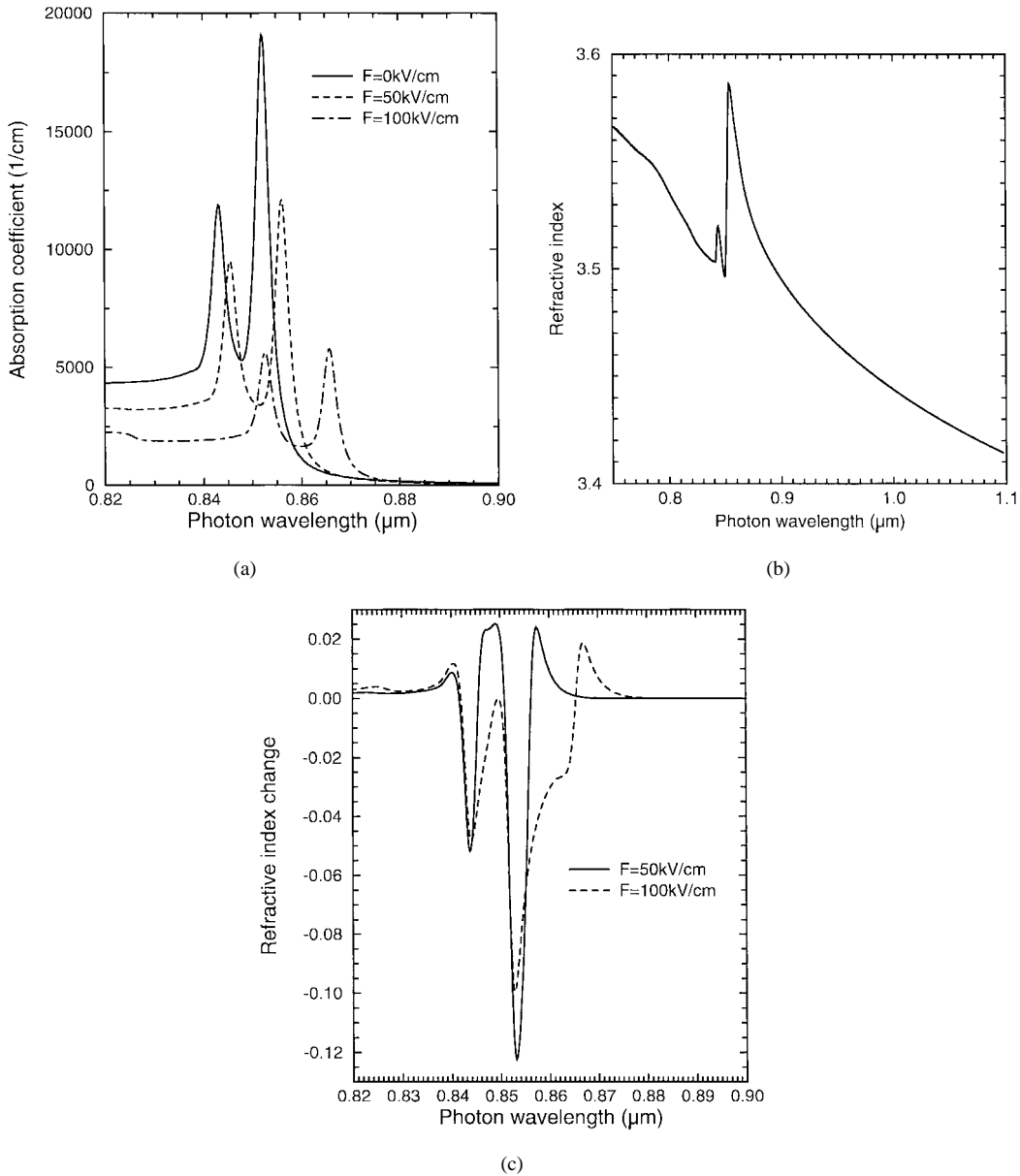


Fig. 3. (a) Absorption spectra of 100-Å/100-Å $\text{Al}_{0.3}\text{Ga}_{0.7}\text{As}$ -GaAs QW's for applied fields of 0 (solid line), 50 kV/cm (dashed line), and 100 kV/cm (dotted-dashed line). (b) Unbiased refractive index spectra of the QW structure. (c) Change of refractive index spectra for applied fields of 50 (solid line) and 100 kV/cm (dash line).

power which overlaps the depletion region of the p-i-n structure, which consists of a QW active region and part of the two (top and bottom) cladding layers, within the entire device structure. Therefore, an efficient modulator requires a large value of Γ . Moreover, a good phase modulator requires low α_{loss} , where α_{loss} is defined as α_{eff} for $F = 0$. The electrical bias required for modulation is also a crucial parameter which indicates the power consumption of the device, which is due to power dissipation in the load resistance of the drive circuit.

E. The p-i-n Junction Depletion Region

The phase modulator uses a reverse bias p-i-n structure to deplete the active region of free carriers. The electric field distribution in the structure is shown in Fig. 4. The electric field and potential of the p-i-n structure are determined by

solving Poisson's equation in one dimension with appropriate boundary conditions [16]

$$-\nabla^2\Theta = \rho/\epsilon \quad (13)$$

where Θ is potential, ρ is charge density and ϵ dielectric constant. Since the dielectric constants are different in each layer of the heterojunction structure, the derivation of the relevant quantities is rather complex. The potential difference (V) across the depletion width is given by $V = \Theta(-x_n) - \Theta(x_p)$ and, by using (13), $\Theta(-x_n)$ and $\Theta(x_p)$ can be expressed in terms of the depletion layer thickness and the carrier density of the p-i-n structure. The integrated form of (13) is expressed as a quadratic equation for the depletion layer width x_m and,

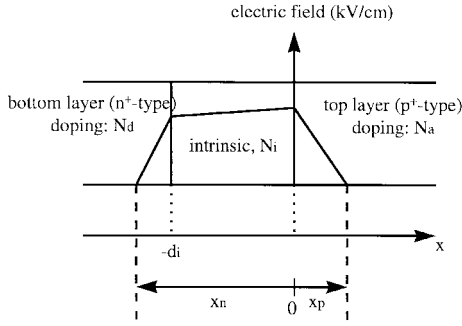


Fig. 4. The electric field profile of the p-i-n phase modulator.

thus, the solution for x_m can be written as

$$x_m = x_n + x_p = \frac{-Q_b \pm \sqrt{Q_b^2 - 4Q_a(Q_c - V/q)}}{2Q_a} \quad (14)$$

where

$$Q_a = \frac{N_n a^2}{2\epsilon_n} + \frac{N_p c^2}{2\epsilon_p}; \quad Q_b = b \left(\frac{N_n a}{2\epsilon_n} + \frac{N_p c}{2\epsilon_p} \right) - \delta$$

$$Q_c = \frac{b^2}{2} \left(\frac{N_n}{\epsilon_n} + \frac{N_p}{\epsilon_p} \right)$$

$$\delta = d_i \left(\frac{N_n a}{\epsilon_n} + \frac{N_p c}{\epsilon_p} \right); \quad a = \frac{N_p}{N_n + N_p}$$

$$b = \frac{d_i(N_p + N_i)}{N_n + N_p}; \quad c = l - a = \frac{N_n}{N_n + N_p}$$

where ϵ is the dielectric constant, N is the dopant concentration, and the subscripts p, i, and n refer to the relevant layers of the p-i-n structure, respectively, d_i is the thickness of the active region, and q is an electronic charge. The average electric field, E , in the depletion region is obtained using $E = V/x_m$, where $V = V(\text{built-in}) - V(\text{applied})$ and $V(\text{built-in})$ is calculated for zero bias voltage. The applied voltage, $V(\text{applied})$, equivalent to the electric field in the depletion layer is then calculated.

F. Breakdown Voltage

Junction breakdown is modeled here by avalanche multiplication [25]. The multiplication factor is derived from [26] to depict the electric field induced increase in hole current. The avalanche breakdown voltage is defined as the voltage when the multiplication factor approaches infinity, which causes the ionization integral to become unity and breakdown is reached and obtained by

$$\int_0^{x_m} \varsigma_h \exp \left[- \int_0^x (\varsigma_h - \varsigma_e) dx' \right] dx = 1 \quad (15)$$

where ς_h and ς_e are the ionization rates for holes and electrons, respectively, and x is the QW growth direction.

III. RESULTS AND DISCUSSIONS

The active region of the modulator consists of undoped multiple periods of 100-Å $\text{Al}_{0.3}\text{Ga}_{0.7}\text{As}$ barriers and 100-

Å-thick GaAs wells. The two structures studied here comprise 0.5- and 1.0- μm -thick QW regions which contain 25 and 50 QW periods, respectively. The effects of the implanted impurities on the confinement of the optical field in these two structures are studied. The implantation parameters, including the projected ion range and standard deviation and the lateral spread of the implanted ions around the mask for different implant energies are taken from [27] and the Al and Ga interdiffusion coefficients are taken from [28].

The top and bottom highly doped p and n $\text{Al}_{0.3}\text{Ga}_{0.7}\text{As}$ cladding layers, which have a dopant concentration of 10^{18} cm^{-3} , are used to form a p-i-n structure, respectively, on an n^+ -GaAs substrate, where the carrier concentration of intrinsic region is 10^{15} cm^{-3} . It is assumed that the implantation-induced IID process has no effect to the electrical properties of the cladding layers. The operating wavelength of this modulator is longer than the bandgap wavelength of the $\text{Al}_{0.3}\text{Ga}_{0.7}\text{As}$ cladding layers and barriers of QW's. Consequently, only that part of the propagating optical wave that interacts with the wells of QW's will be absorbed and strong optical confinement is required to maximize this interaction and increase $\Delta\theta_N$ of the modulator. Under reverse bias, the QW's are completely depleted and the modulation of the optical beam in the depletion region is assumed to be due to the quantum-confined Stark effect. It is considered that if the intensity of optical light source is weak, i.e., $< 25 \mu\text{W}$ [29], with a low carrier concentration in intrinsic region (10^{15} cm^{-3}), the carrier effect to bound state absorption and exciton state absorption are very small, as reported in [30] and [31], respectively, and thus can be neglected. The performance of the modulator for applied fields (F) of 50 and 100 kV/cm are reported here.

A. Operating Wavelength

The selection of λ_{op} is important for high modulation performance, including a large $\Delta\theta_N$, a large β_{mod} , i.e., a high refractive index change together with low absorption change for phase modulator, a low applied voltage, and a low α_{loss} . However, there is a tradeoff between these various parameters. For example, a Δn as high as 0.12 can be obtained for an applied field of 50 kV/cm at λ_{op} of 0.854 μm [see Fig. 3(c)], although α_{loss} is very high, $> 7200 \text{ cm}^{-1}$. There is a tradeoff between high refractive index change and high absorption loss. At this operating wavelength, $\Delta\alpha_{\text{eff}}$ is also too high (5600 cm^{-1}) and, thus, from (6), β_{mod} is very small and below 1 ($\ll 10$). As a consequence, the phase modulator is not suitable for operation at this wavelength. On the other hand, low α_{loss} ($< 500 \text{ cm}^{-1}$) can be obtained at wavelengths far enough away from the unbiased exciton absorption peak, i.e., above 0.86 μm . When the operating wavelength increases, both α_{loss} and Δn reduces [see Fig. 3(a) and (c), respectively]. Consequently, $0.868 \mu\text{m} > \lambda_{\text{op}} > 0.86 \mu\text{m}$ and $0.878 \mu\text{m} > \lambda_{\text{op}} > 0.87 \mu\text{m}$ should be used for $F = 50 \text{ kV/cm}$ and $F = 100 \text{ kV/cm}$, respectively, to achieve $\Delta\theta_N \geq 0.59 \text{ rad/V}\cdot\text{mm}$ of the existing device [25], for which acceptable values of α_{loss} ($< 500 \text{ cm}^{-1}$) can be obtained.

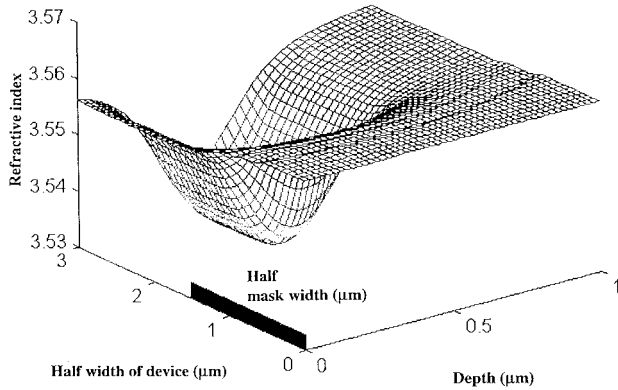


Fig. 5. The refractive index profile of the phase modulator.

B. Impurity Distribution versus Mode Field

The refractive index profiles are obtained for the designed value of λ_{op} to ensure single-mode operation. The transverse refractive index profiles of the waveguide structure are inhomogeneous and are highly dependent on the impurity concentration, the implanted ion energy, the annealing temperature, and time. The refractive index profile of half of the transverse device structure for λ_{op} of $0.863 \mu\text{m}$ is shown in Fig. 5. Since the concentration of impurities peak at a depth of $0.5 \mu\text{m}$, the refractive index of the lateral cladding region is a minimum at such a depth. However, the active region of the device, which is protected by the mask, provides a relatively uniform refractive index profile for phase modulation. Moreover, it can be observed that the refractive index of the interface between lateral cladding and active region from 1.5 to $2.0 \mu\text{m}$ stripe width is graded rather than an abrupt interface.

The ion dose modeled here is $2.5 \times 10^{13} \text{ ion/cm}^2$ so that the lattice damage levels are minimized to reduce the damage-induced waveguide loss and to retain the electrooptical properties of the material. The implanted ion energy is optimized to achieve maximum optical confinement. The optimized conditions and mode field for the $0.5\text{-}\mu\text{m}$ QW structure are an ion energy of 650 keV and a $\Gamma > 0.75$. Fig. 6 shows that the peak of the mode field coincides with the peak of the impurity profile at the center of the QW guiding layer.

C. Single Mode Operation

The results show that using the selected ion energy and dose, a range of refractive index profiles can produce single-mode modulation at the selected operation wavelengths. This is best illustrated by plotting the normalized propagation constant as a function of annealing time [see Fig. 7] for $0.5\text{-}\mu\text{m}$ structures and $\lambda_{op} = 0.863 \mu\text{m}$, which shows the variation of the guiding properties of the QW waveguide, in terms of the normalized propagation constant, for different annealing times. The mode cutoff intervals SMF0 and SMF50 correspond to the ranges in which only single-mode waveguides are formed for applied electric fields of 0 and 50 kV/cm , respectively.

The applied electric field modifies the refractive index profile and thus the normalized propagation constant of the guided mode, as shown in Fig. 7. In the case of $0.5\text{-}\mu\text{m}$ active

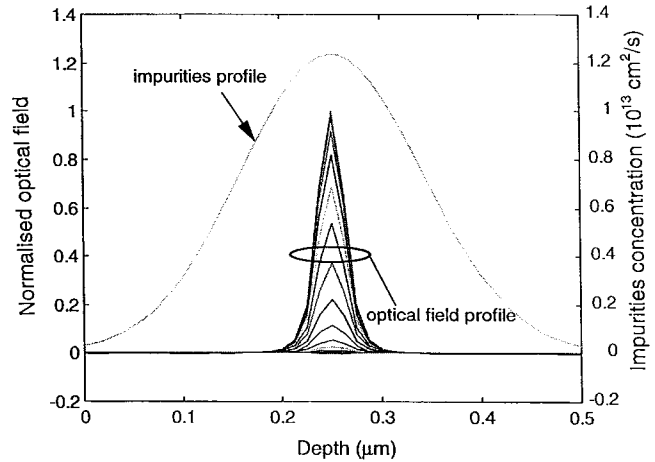


Fig. 6. The impurity profile and mode field profile of the phase modulator.

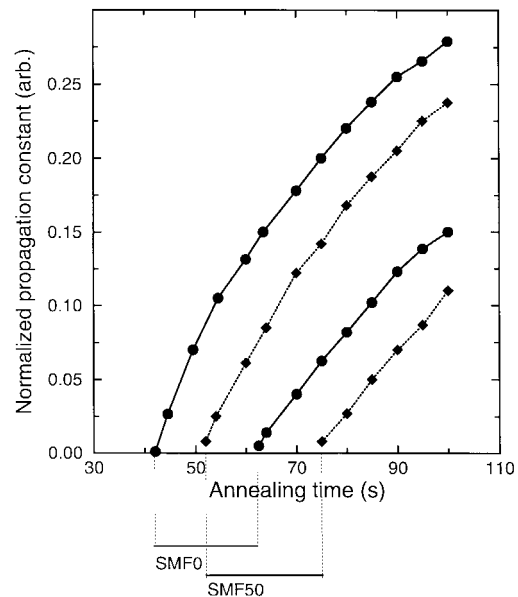


Fig. 7. The variation of the normalized propagation constant with annealing time, showing the single-mode range of operation for various applied field values. The intervals SMF0 and SMF50 corresponds to the ranges in which the waveguides behave as single-mode guides for an applied field of 0 and 50 kV/cm for 25-period QW structure and λ_{op} of $0.863 \mu\text{m}$.

region, $\lambda_{op} = 0.863 \mu\text{m}$ and applied field $F = 0$, the interval (SMF0) covers the annealing time from 42 to 62.5 s . However, when the applied field is increased to 50 kV/cm , the interval (SMF50) shifts to longer annealing times which range from 52 to 74.5 s , outside which the waveguide will change from a single mode to multimode device at $\lambda_{op} = 0.863 \mu\text{m}$. To maintain single-mode operation, only the overlapping region between the two mode cutoff intervals of the two selected applied fields should be used. For instance, for an operation with $F = 0$ and $F = 50 \text{ kV/cm}$ in the case of Fig. 7, the overlapping region between SMF0 and SMF50, i.e., annealing time between $52\text{--}64 \text{ s}$, should be used for a single-mode phase modulator. Here, the annealing time at the mid-point of the overlapping region is used for the design of the ion-implanted phase modulator. By plotting a similar diagram for the same $0.5\text{-}\mu\text{m}$ QW structure, single-mode operation of

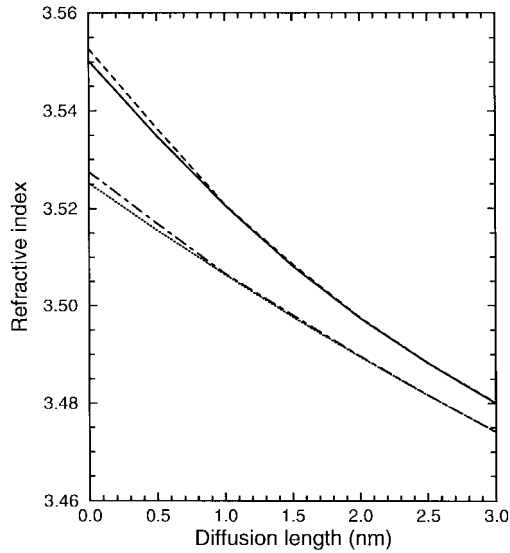


Fig. 8. The variation of the refractive index with diffusion length (L_d) for fields of 0 kV/cm (solid line) and 50 kV/cm (dashed line) for λ_{op} of 0.863 μm , and for fields of 0 kV/cm (dotted line) and 100 kV/cm (dot-dashed line), respectively, for λ_{op} of 0.873 μm .

phase modulation can also be obtained at $\lambda_{op} = 0.873 \mu\text{m}$ with $F = 0$ and 100 kV/cm while the 1- μm QW structure can only operate with 0 and 50 kV/cm for single-mode operation at $\lambda_{op} = 0.863 \mu\text{m}$.

D. Metal Contact Width

The width of the metal contact influences the refractive index change in DFQW's under the two biases (50 and 100 kV/cm). Since the width of the metal contact is a few micrometers and the depth of the active region is $\leq 1 \mu\text{m}$, the electric field in the QW region is uniform and fringing fields have been neglected. When $L_d \geq 8 \text{ nm}$, the refractive index of the DFQW's remains approximately constant for applied field $F = 50$ and 100 kV/cm [see Fig. 8]. The main reason is that when L_d increases, the transition energy of the QW structure increases [16], the DFQW exciton absorption peaks are blue shifted away from the selected λ_{op} of 0.863 μm for $F = 50$ kV/cm and 0.873 μm for $F = 100$ kV/cm, i.e., the exciton effect becomes very small at these two operation wavelengths. As shown in Fig. 8, for the two selected wavelengths, the refractive index change due to exciton reduces with L_d . Consequently, when the 100-Å/100-Å $\text{Al}_{0.3}\text{Ga}_{0.7}\text{As}$ -GaAs QW structure is diffused with $L_d \geq 8 \text{ nm}$, the refractive index change at both λ_{op} of 0.863 and 0.873 μm are too small to be considered.

To develop a high-performance phase modulator, the width of the metal contact needs to be sufficiently large to cover the graded waveguide/cladding interface which is greater than the width of the waveguide mask after interdiffusion, for $L_d < 8 \text{ nm}$, otherwise a sharp jump of the refractive index under an applied field will be obtained below the metal contact edge [see Fig. 9]. The width of the metal contact here is the same as that of the waveguide mask. When an applied field of 50 kV/cm is used, the refractive index of the active region increases and, thus, produces an abrupt change of refractive

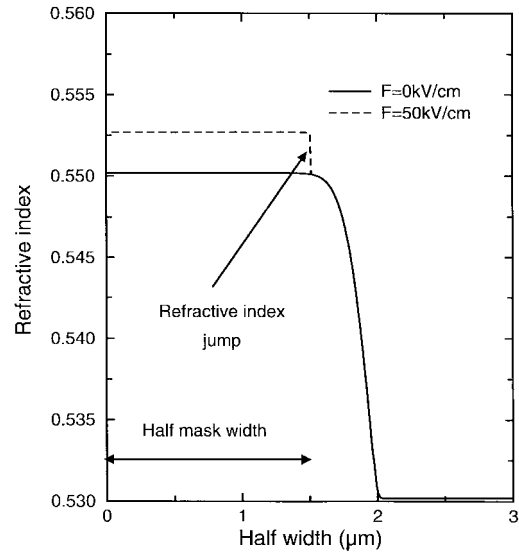


Fig. 9. Refractive index profile, with and without the applied electric field across AB in Fig. 1. The width of the metal contact is the same as that of the waveguide mask in this structure.

TABLE I
MODULATION PROPERTIES OF THE TWO CAVITY STRUCTURES

QWs thickness (μm)	0.5				1.0	
	0.863	0.867	0.873	0.877	0.863	0.867
λ_{op} (μm)	0.863	0.867	0.873	0.877	0.863	0.867
bias field (kV/cm)	50	50	100	100	50	50
bias voltage (V)	2.54	2.54	5.06	5.06	5.04	5.04
depletion width (μm)	0.507	0.507	0.512	0.512	1.06	1.06
Γ	0.80	0.79	0.78	0.77	0.86	0.87
$\Delta n_{eff} (\times 10^{-3})$	2.26	0.31	2.03	0.42	2.48	0.35
$\Delta\theta_N$ (rad/Vmm)	6.48	0.89	2.88	0.60	3.58	0.50
$\alpha_{loss} (\text{cm}^{-1})$	302.7	174.6	111.6	85.2	332.3	195.6
$\Delta\alpha_{eff} (\text{cm}^{-1})$	107.6	8.1	76	5.2	117.3	9.0
β_{mod}	3.1	5.5	3.8	11.6	3.1	5.6

index at the edge of the metal contact. This abrupt change causes a discontinuity in the optical field propagation constant and reduces the modulation properties. The refractive index of the DFQW with $L_d < 8 \text{ nm}$ will change, due to the applied field, at the selected operation wavelengths [see Fig. 8]. Hence, the metal contact should extend at least to cover the DFQW with $L_d < 8 \text{ nm}$ to avoid the abrupt refractive index change and thus the discontinuity of optical field. As a consequence, a metal contact width of 4 μm , which is slightly larger than the waveguide mask width (3 μm), is used here.

E. Modulation Performance

Several parameters are used to characterize the performance characteristics of the modulator (see Table I). A large phase change with $\Delta\theta_N > \pi/2 \approx 1.57 \text{ rad/V}\cdot\text{mm}$ can be obtained at the selected λ_{op} 's of 0.863 and 0.873 μm for $F = 50$ and 100 kV/cm, respectively, in the 0.5- μm structure and 0.863 μm for $F = 50$ kV/cm in the 1- μm structure. Their α_{loss} values are also $< 500 \text{ cm}^{-1}$. For the 0.5- μm active region, this value reduces to 111.6 cm^{-1} when the applied field increases to 100 kV/cm because the λ_{op} can be further away from the unbiased HH exciton peaks, as compared to that for $F = 50$ kV/cm.

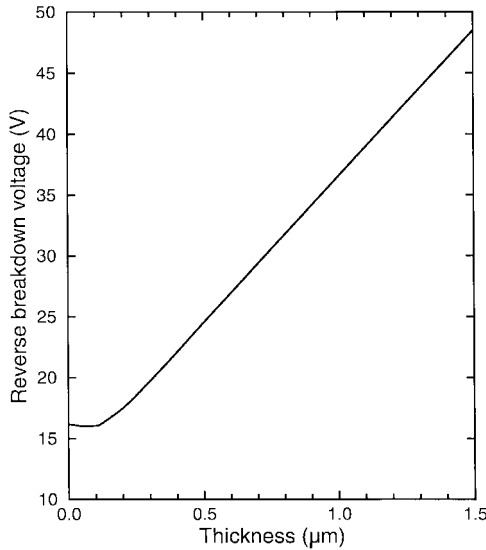


Fig. 10. The variation of the breakdown voltage with QW active region thickness.

For the 1 μm QW active region, the total phase modulation for 50 kV/cm is 18.1 rad/mm, which is larger than that for the 0.5- μm QW active region (16.4 rad/mm) and it is due to the greater optical confinement in the 1.0- μm QW active region, where twice the number of QW's contribute to the modulation mechanism. However, the operation of the 1.0- μm QW structure requires approximately twice the applied voltage as compared to that of 0.5- μm QW structure. This makes the $\Delta\theta_N$ of the 1.0- μm QW structure weaker than that of the 0.5- μm QW structure, i.e., the 0.5- μm QW structure provides a more efficient modulation.

In both structures, β_{mod} is low with values of 3.1 and 3.8 for λ_{op} of 0.863 and 0.873 μm , respectively. In order to increase β_{mod} , a longer wavelength is used, such as for $F = 50$ kV/cm when λ_{op} is increased to 0.867 μm and β_{mod} increases to ~ 5.5 . This improvement of β_{mod} is mainly due to the reduction of $\Delta\alpha_{\text{eff}}$, as shown in Table I, but the penalty is a reduction of $\Delta\theta_N$. This case clearly shows the tradeoff between $\Delta\theta_N$ and $\Delta\alpha_{\text{eff}}$. A larger β_{mod} can be obtained using $F = 100$ kV/cm when λ_{op} increases from 0.873 to 0.877 μm where β_{mod} increases to 11.6. The $\Delta\theta_N$ here is $0.6 \sim 34.4^\circ$ rad/Vmm and this phase change is compatible with the existing device [25].

For a dc offset used in the phase modulator, larger phase changes may be obtained [32], although the breakdown voltage of the structure determines the maximum operating voltage of the device. The breakdown voltage for the 0.5- and 1- μm devices are 25 and 37 V, respectively (see Fig. 10).

IV. CONCLUSION

Two waveguide-type phase modulators with 0.5- and 1- μm QW active regions using masked ion implantation to produce lateral confinement have been investigated theoretically. These devices are designed for single-mode operation at a wavelength of 0.867 μm for an applied field of 50 kV/cm and 0.877 μm for 100 kV/cm, where interdiffusion can be used to tune the propagating modes of the device.

The metal contact width is made deliberately larger than the waveguide width to avoid the discontinuity of refractive index profile at the lateral cladding/core interface. The design of a single-mode phase modulator with strong optical confinement requires the peak ion concentration to be at the center of the guiding layer. Moreover, the annealing time is selected to be within the range required to achieve single-mode operation for the two applied field values. Low impurity concentrations are also required to minimize lattice damage and retain the electrooptical properties of the material.

Comparing the modulation properties of 0.5- and 1- μm QW structures, the 1.0- μm structure can provide higher optical confinement and larger total phase change per unit length. The 0.5- μm structure can operate with either 0 and 50 kV/cm or with 0 and 100 kV/cm. The more important comparison is $\Delta\theta_N$ of the two structures. The 0.5- μm structure can provide more efficient modulation since its value of $\Delta\theta_N$ is approximately twice that of the 1.0- μm structure. β_{mod} and α_{loss} of the 0.5- μm structure can be further increased and reduced, respectively, by increasing the applied field from 50 to 100 kV/cm since the longer λ_{op} can be used. It is important to note that a β_{mod} of 11.6, which is obtained for a field of 100 kV/cm, is large enough for a good phase modulator. The results are a guideline for the development of an optical phase modulator using lateral confinement provided by impurity-induced disordering, which is also useful when these devices are used in photonic integrated circuits.

REFERENCES

- [1] G. W. Yoffe, J. Brubach, W. C. Van der Vleuten, F. Karouta, and J. H. Wolter, "Low voltage hetero-nipi wavelength modulators," *Trans. Electron Devices*, vol. 40, pp. 2144–2147, 1994.
- [2] S. Yoshida, Y. Tada, I. Kotaka, and K. Wakita, "InGaAs/InAlAs multi-quantum well electroabsorption phase modulator module," *Electron. Lett.*, vol. 30, pp. 1795–1796, 1994.
- [3] A. Ramdane, P. Krauz, E. V. K. Rao, A. Hamoudi, A. Ougazzaden, D. Robein, A. Gloukhan, and M. Carré, "Monolithic integration in InGaAs-InP strained-layer distributed feedback laser and external modulator by selective quantum-well interdiffusion," *IEEE Photon. Technol. Lett.*, vol. 7, pp. 1016–1018, 1995.
- [4] B. L. Olmsted and S. N. Houde-Walter, "Dependence of Al-Ga interdiffusion in AlGaAs on stoichiometry between Ga-rich and As-rich solidus limits," *Appl. Phys. Lett.*, vol. 60, pp. 368–370, 1992.
- [5] K. Kash, B. Tell, P. Grabbe, E. A. Dobisz, H. G. Graighead, and C. M. Tamargo, "Aluminum ion-implantation enhanced intermixing of GaAs-AlGaAs quantum-well structures," *J. Appl. Phys.*, vol. 63, pp. 190–194, 1988.
- [6] B. L. Weiss, I. V. Bradley, N. J. Whitehead, and J. S. Roberts, "Disordering of AlGaAs/GaAs quantum well structures using low doses oxygen implantation," *J. Appl. Phys.*, vol. 71, pp. 5715–5719, 1992.
- [7] D. G. Deppé, L. H. Guido, N. Holonyak, Jr., K. C. Hsieh, R. D. Burnham, D. L. Thornton, and E. L. Paoli, "Stripe-geometry quantum well heterostructure $\text{Al}_x\text{Ga}_{1-x}\text{As}$ -GaAs lasers defined by defect diffusion," *Appl. Phys. Lett.*, vol. 49, pp. 510–512, 1986.
- [8] C. Vien, M. Schneider, D. Maily, R. Planel, H. Launois, H. Y. Marzin, and B. Descouts, "Optical characterization of selectively intermixed GaAs/GaAlAs quantum wires by Ga⁺ masked implantation," *J. Appl. Phys.*, vol. 70, pp. 1444–1450, 1991.
- [9] P. J. Poole, S. Charbonnesu, M. Dion, G. C. Aers, M. Buchana, R. D. Golderb, and I. V. Mitchell, "Demonstration of an ion-implanted wavelength-shifted quantum-well laser," *IEEE Photon. Technol. Lett.*, vol. 8, pp. 16–18, 1996.
- [10] M. Ghisoni, G. Parry, M. Pate, G. Hill, and J. Roberts, "Post growth fabrication of GaAs/AlGaAs reflection modulators via impurity free disordering," *Jpn. J. Appl. Phys.*, vol. 30, pp. L1018–L1020, 1991.
- [11] E. Kapon, N. G. Stoffel, E. A. Dobisz, and R. Bhat, "Birefringent channel waveguides defined by impurity-induced superlattice disordering," *Appl. Phys. Lett.*, vol. 52, pp. 351–353, 1988.

- [12] P. J. Bradley and G. Parry, "Optimized multiple quantum well phase modulator," *Electron. Lett.*, vol. 25, pp. 1349–1350, 1989.
- [13] W. C. H. Choy, E. H. Li, and J. Micallef, "The polarization insensitive electro-absorptive and -refractive modulation by utilizing InGaAsP/InP interdiffused quantum well," *IEEE J. Quantum Electron.*, vol. 33, pp. 1316–1323, 1997.
- [14] E. H. Li and W. C. H. Choy, "Modulation properties of InGaAsP/InP diffused quantum wells," *J. Appl. Phys.*, Oct. 1997.
- [15] J. Micallef, E. H. Li, and B. L. Weiss, "Effect of interdiffusion on the polarization dependent refractive index of a strained InGaAs/GaAs quantum well," *Appl. Phys. Lett.*, vol. 62, pp. 3164–3166, 1993.
- [16] W. C. H. Choy and E. H. Li, "The applications of interdiffused quantum well in normally-on electro-absorptive Fabry–Perot reflection modulation," *IEEE J. Quantum Electron.*, vol. 33, pp. 382–393, 1997.
- [17] S. Adachi, "Optical-properties of $\text{Al}_x\text{Ga}_{1-x}\text{As}$ alloys," *Phys. Rev. B*, vol. 38, pp. 12345–12352, 1988.
- [18] G. J. Sonek, J. M. Ballantyne, Y. J. Chen, G. M. Carter, S. W. Brown, E. S. Koteles, and J. P. Slaerno, "Dielectric properties of GaAs/AlGaAs multiple quantum well waveguides," *IEEE J. Quantum Electron.*, vol. QE-22, pp. 1015–1018, 1986.
- [19] E. H. Li and W. C. H. Choy, "The electro-optic effect in an interdiffusion induced AlGaAs/GaAs quantum well," *IEEE Photon. Technol. Lett.*, vol. 7, pp. 881–883, 1995.
- [20] T. Y. Tan, U. Gösele, and S. Yu, "Point defects, diffusion mechanisms, and superlattice disordering in gallium arsenide-based materials," *Critic. Rev. Solid State Mater. Sci.*, vol. 17, pp. 47–106, 1991.
- [21] J. Cibert and P. M. Petroff, "Carrier confinement potential in quantum-well wires fabricated by implantation-enhanced interdiffusion in the GaAs– $\text{Ga}_{1-x}\text{Al}_x\text{As}$ system," *Phys. Rev. B*, vol. 36, pp. 3243–3246, 1987.
- [22] E. H. Li, B. L. Weiss, and K. S. Chan, "Effect of interdiffusion on the subbands in an $\text{Al}_x\text{Ga}_{1-x}\text{As}/\text{GaAs}$ single-quantum-well structure," *Phys. Rev. B*, vol. 46, pp. 15180–15192, 1992.
- [23] S. J. Hewlett and F. Ladouceur, "Fourier deposition method applied to mapped infinite domains: Scalar analysis of dielectric waveguides down to modal cutoff," *J. Lightwave Technol.*, vol. 13, pp. 375–383, 1995.
- [24] T. Hausken, R. H. Yan, R. I. Simes, and L. A. Coldren, "Relating the chirp parameter to the number of quantum wells in GaAs/AlGaAs waveguide modulators," *Appl. Phys. Lett.*, vol. 55, pp. 718–720, 1989.
- [25] S. M. Sze, *Physics of Semiconductor Devices*, 2nd ed. New York: Wiley, 1981, ch. 2, p. 99.
- [26] ———, *Physics of Semiconductor Devices*, 2nd ed. New York: Wiley, 1981, ch. 2, p. 195.
- [27] J. F. Gibbons, W. S. Johnson, and S. W. Mylroie, *Projected Range Statistics: Semiconductors and Related Materials*, 2nd ed. Stroudsburg, PA: Dowden, Hutchinson & Ross, 1975.
- [28] J. Cibert, P. M. Petroff, D. J. Werder, S. J. Pearton, A. C. Gossard, and J. H. English, "Kinetics of implantation enhanced interdiffusion of Ga and Al at GaAs– $\text{Ga}_x\text{Al}_{1-x}\text{As}$ interfaces," *Appl. Phys. Lett.*, vol. 49, pp. 223–225, 1986.
- [29] M. Glick, F. K. Reinhart, G. Weimann, and W. Schlapp, "Quadratic electro-optic light modulation in a GaAs/AlGaAs multiquantum well heterostructure near the excitonic gap," *Appl. Phys. Lett.*, vol. 48, pp. 989–991, 1986.
- [30] E. H. Li, "The effect of carriers on the optical properties of Al-GaAs/GaAs interdiffused quantum well lasers," *SPIE Proc.*, vol. 2886, pp. 151–160, 1996.
- [31] B. M. Ashkinadze, E. Linder, E. Cohen, A. Ron, and L. N. Pfeiffer, "Free-carrier effect on exciton dynamics in GaAs/ $\text{Al}_x\text{Ga}_{1-x}\text{As}$ quantum wells," *Phys. Rev. B*, vol. 51, pp. 1938–1941, 1995.
- [32] J. E. Zucher, T. L. Hendrickson, and C. A. Borrus, "Low voltage phase modulation in GaAs/AlGaAs quantum well optical waveguides," *Electron. Lett.*, vol. 24, pp. 112–113, 1988.

Wallace C. H. Choy received the B.Sc. degree in applied physics from the Baptist University of Hong Kong in 1994 and the M.Phil. degree in electronic engineering from the University of Hong Kong in 1996. His thesis was concerned with the modeling of optical properties of interdiffusion modified quantum-well structures for modulation devices. He is currently pursuing the Ph.D. degree in electronic engineering at the University of Surrey, Surrey, U.K.

He currently holds a Croucher Foundation Scholarship. His main research topics include the influence of acoustic waves in quantum-well materials and acoustooptic devices for optoelectronics applications.

Mr. Choy was awarded the Sir Edward Youde Memorial Fellowship and a Postgraduate Studentship award while performing his graduate work.

Bernard L. Weiss (S'72–M'74–SM'94) received the B.Sc. degree in electrical engineering and the Ph.D. degree in solid-state electronics from the University of Newcastle upon Tyne, U.K., in 1971 and 1974, respectively.

He was awarded an SRC Personal Post-Doctoral Research Fellowship for the study of anodic oxides on GaAs in 1975, and in 1977 he moved to University College London as a Research Fellow, where he worked on acoustic nondestructive testing. In 1979, he was appointed a Lecturer in Electronic Engineering at the University of Surrey, U.K., where he set up research in integrated optical devices in LiNbO_3 . He was promoted to Senior Lecturer, Reader, and Professor in 1986, 1993, and 1996, respectively. His research is concerned with modeling the optical properties of III–V semiconductor quantum-well structures and devices and optoelectronic devices in silicon-based materials and photosensitivity in glass. In 1991, he spent six months sabbatical leave at the University of Cincinnati, Cincinnati, OH, in 1994–1995 he was a DFG Visiting Professor at the Technische Hochschule Darmstadt, Germany, and he is an Honorary Professor at the University of Hong Kong.

Dr. Weiss is a fellow of the Institution of Electrical Engineers (IEE, U.K.) and the Institute of Physics (U.K.). He is Chair of the IEE Scholarships Committee, a member of several other IEE committees, and editor of the IEE EMIS book series. He was awarded the Medal of the University of Warsaw for his contributions to the TEMPUS project.

E. Herbert Li (S'87–M'88–SM'95) received the M.Phil. degree in applied mathematics and electronic engineering from the University of Hong Kong and the Ph.D. degree in electronic engineering from the University of Surrey, Surrey, U.K.

He worked for the Kirsten Aeronautical Laboratory, Seattle, WA (1979–1980). He joined KK Engineering Company, Hong Kong, as an Engineer (1981–1986) and Micro Systems, Hong Kong, as a Manager (1986–1988). He was a Member of Faculty at the City University of Hong Kong (1988–1990). He joined the National Ion Implantation Facility at the Department of Electrical and Electronic Engineering, University of Surrey (1990–1993). He is currently a Member of Faculty and Leader of the Optoelectronics Group, which consists of a team of 10 researchers, at the Department of Electrical and Electronic Engineering, University of Hong Kong (1994–present). He is an Adjunct Professor of the Institute of Semiconductors, Shandong Normal University, China, and a Visiting Faculty Member at the University of Waterloo, Canada. His current research interests are mainly concerned with optoelectronic device fabrication, modeling, and characterization, and in particular interdiffusion-induced modification of quantum-well structures for the advanced performance and integration of optoelectronic devices. Since 1990, he has published over 100 international technical papers, two book chapters, and three books in the above areas. He served on both the Technical Program and International Advisory Committees of OECC in 1996 (Japan) and 1997 (Korea). He is an Editor of the *International Journal of Optoelectronics*.

Dr. Li is a "Distinguished Lecturer" of the IEEE Electron Device Society (EDS) for 1997, and he is an AdCom *ex officio* member and EDS Meeting Committee member of the IEEE. He received the J. Langham Thompson Premium Prize in 1992 from the Institution of Electrical Engineers (U.K.) and the Distinguished Pioneering Projects Award in 1989 from HKCSS (Hong Kong). His biography is published in *Who's Who in Science and Engineering*.